

# Second Generation Pleated Pneumatic Artificial Muscle and Its Robotic Applications

Björn Verrelst, Ronald Van Ham, Bram Vanderborght, Dirk Lefeber  
& Frank Daerden

Vrije Universiteit Brussel, Department of Mechanical Engineering, Pleinlaan 2, 1050 Brussels, Belgium  
Björn Verrelst: tel: +32-2-629.28.63, fax: +32-2-629-28-65, e-mail: bjorn.verrelst@vub.ac.be  
Ronald Van Ham: tel: +32-2-629.28.62, fax: +32-2-629-28-65, e-mail: ronald.van.ham@vub.ac.be  
Bram Vanderborght: tel: +32-2-629.31.81, fax: +32-2-629-28-65, e-mail: bram.vanderborght@vub.ac.be  
Dirk Lefeber: tel: +32-2-629.28.64, fax: +32-2-629-28-65, e-mail: dlefeber@vub.ac.be  
Frank Daerden: tel: +32-2-629.28.63, fax: +32-2-629-28-65, e-mail: fdaerden@vub.ac.be  
<http://lucy.vub.ac.be>

## Abstract

This paper reports on the second generation of the Pleated Pneumatic Artificial Muscle (PPAM) which has been developed to extend the life span of its first prototype. This type of artificial was developed to overcome dry friction and material deformation which is present in the widely used McKibben type of artificial muscle. The essence of the PPAM is its pleated membrane structure which enables the muscle to work at low pressures and at large contractions. There is a growing interest in this kind of actuation for robotics applications due to its high power to weight ratio and the adaptable compliance, especially for legged locomotion and robot applications in direct contact with a human.

This paper describes the design of the second generation PPAM, for which specifically the membrane layout has been changed. In function of this new layout the mathematical model, developed for the first prototype, has been reformulated. This paper gives an elaborate discussion on this mathematical model which represents the force generation and enclosed muscle volume. Static load tests on some real muscles, which have been carried out in order to validate the mathematical model, are then discussed.

Furthermore are given two robotic applications which currently use these pneumatic artificial muscles. One is the biped Lucy and the another one is a manipulator application which works in direct contact with an operator.

**Keywords:** Compliant Actuation, Pneumatic Artificial Muscle, Mathematical Modelling.

## 1 Introduction

A pneumatic artificial muscle (PAM) is essentially a volume, enclosed by a reinforced membrane, that expands radially and contracts axially when inflated with pressurized air. Hereby the muscle generates a uni-directional pulling force along the longitudinal axis. When neglecting

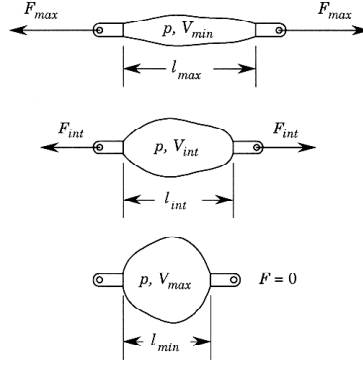


Figure 1: Working principle of a pneumatic artificial muscle [2]

the membrane's material deformation and the low inertial muscle properties, the generated force is expressed as [1, 2]:

$$F = -p \frac{dV}{dl} \quad (1)$$

with  $p$  the gauge pressure inside the muscle,  $dV$  enclosed muscle volume changes and  $dl$  actuator length changes. The volume of the actuator increases with decreasing length until a maximum volume is reached. At maximum contraction, forces become zero, and at low contraction these forces can be very high. Figure 1 gives the working principle of a PAM at constant pressure. The changing force as a function of contraction at constant pressure is essentially different compared to standard pneumatic cylinders, for which the generated force does not change at constant pressure. For these devices the generated force is proportional to the piston area on which the internal pressure works, consequently the force does not change with piston position at constant pressure.

Depending on the geometry and type of the membrane, the specific force characteristic alters. Several concepts of PAM have been developed over time, some examples are the Romac muscle [3], the Baldwin muscle type [4], and more recently a muscle with Kevlar reinforced fibers developed in Japan [5]. The best know artificial muscle type is the so called McKibben muscle. This muscle was introduced by McKibben for orthotic applications in the fifties [6]. Several forms of this type of muscle have actually been commercialized by different companies such as Bridgestone Co. [7], the Shadow Robot Company [8], Merlin Systems Cooperation [9] and Festo [10]. More and more interest for these actuators is growing and several groups all over the world use McKibben like muscles in various robotic and medical applications [11, 12, 13, 14, 15, 16, 17, 18, 19].

In figure 2 the concept of the McKibben muscle is given. It contains a rubber inner tube which will expand when inflated, while a braided sleeving transfers tension. Inherent to this design are dry friction between the netting and the inner tube and deformation of the rubber tube. Typical working pressure values range from 1 to 5 bar and more. Due to a threshold of pressure which depends on the rubber characteristics, these muscles do not function properly at low pressures.

To avoid friction and deformation of the rubber material, the Pleated Pneumatic Artificial Muscle (PPAM) has been designed by Daerden [2] at the department of Mechanical Engineering at the Vrije Universiteit Brussel. The membrane of this muscle is arranged into radially laid out folds that can unfurl free of radial stress when inflated. Figure 3 shows the working principle of the PPAM. The membrane is a fabric made of an aromatic polyamide such as Kevlar to which a thin liner is attached in order to make the membrane airtight. The high tensile longitudinal

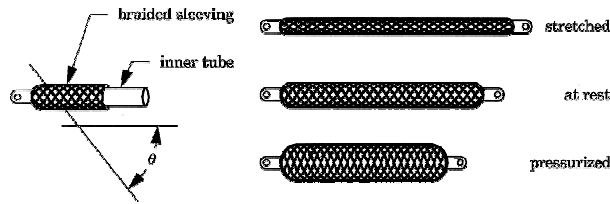


Figure 2: Drawing of the McKibben type muscle [2]

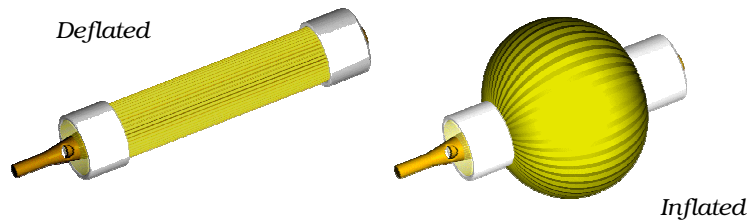


Figure 3: CAD drawing of the deflated and inflated state of the PPAM

fibres of the membrane transfer tension, while the folded structure allows the muscle to expand radially. The folded membrane is positioned into two end fittings which close the muscle and provide tubing to inflate and deflate the enclosed volume. The end fittings are constructed with a circular inner teeth structure to position and align each fold of the membrane, while an outer aluminium ring prevents the membrane of expanding at the end fittings. An epoxy resin fixes the membrane to the end fittings.

Due to its specific design, the PPAM can easily work at pressures as low as 20 mbar. For lifetime considerations of the membrane, the upper limit of the working pressure is set to a maximum 4 bar gauge pressure. Muscle contraction can be more than 40%, depending on its original dimensions (theoretically 54% for a infinitely thin muscle). The muscle prototype built by Daerden [2] has a weight of about 100 gr while it can generate forces up to 5 kN.

## 2 PPAM: adapted design

One of the drawbacks of the first PPAM prototype is its limited lifetime. In Daerden's work, the PPAM design focussed on improving the muscle performance, while studying basic control techniques for an unloaded rotative joint. Extensive usage of the muscles, for example as an actuator for a bipedal walking robot, was however not immediately considered. For any experimental platform the lifespan of the muscle is crucial for obvious reasons. Apart of the interesting scientific aspects related to a study of the PPAM, such a muscle will be economically lucrative, if it can be produced at a reasonable price and has a sufficient lifespan.

### 2.1 Second generation PPAM

One of the causes of the limited muscle lifespan is the overlap used to make a cylindrical pleated membrane. The membrane of the former prototype is folded while starting from a flat woven fabric. The result of the folding process was a flat pleated membrane, and to create a circular

shape, one or two folds are glued together with an overlap. During operation, stresses on the interface between the two overlapped membrane pieces create weakened attachments. The pressurized air finds its way through these weakened spots, which results in leakage. To avoid this, the folding production process was changed. Instead of the folded overlap, the folding now starts from an airtight cylindrical fabric in which the folds are created afterwards.

The toothed inner metal tube of the end fittings of the original prototype requires a lot of machining. Additionally, a large amount of operations are required to position the pleated membrane, fold by fold, in the tooth holes. The idea is to replace this complex end fitting by a straightforward aluminium basin in which the membrane is fixed by the same epoxy resin. The folds are not deliberately aligned, but are assumed to lie already parallel after the improved folding process. The epoxy keeps the pleated membrane in place.

One of the major changes is made to the membrane layout itself. The most important reason for a shorter lifespan, was an incorrect bulging of the pleated membrane. In figure 3 the folds are assumed to unfold evenly, but for a real muscle this was hardly the case. It was witnessed that the membrane is not evenly unfolding, which causes extra parallel stresses on the Kevlar fabric and its airtight coating, especially at the top of each fold. It was observed that the axial Kevlar fibres on each top tend to move towards the bottom of its respective crease, leaving a gap at the top. This of course weakens these spots and facilitates the pressurized air to induce leakage. As a solution to this the membrane composition is changed by only using high tensile stiffness fibres positioned at the bottom of each crease, while another more flexible fabric is used to create the folded membrane structure and keep the pressurized air inside the muscle. The flexible fabric is a simple woven polyester cloth, which is made airtight by a polymer liner. This structure is folded and in each crease a yarn of high-tensile Kevlar fibres is responsible for transferring the large axial tension. Figure 4 depicts the complete straightforward construction of the new muscle.

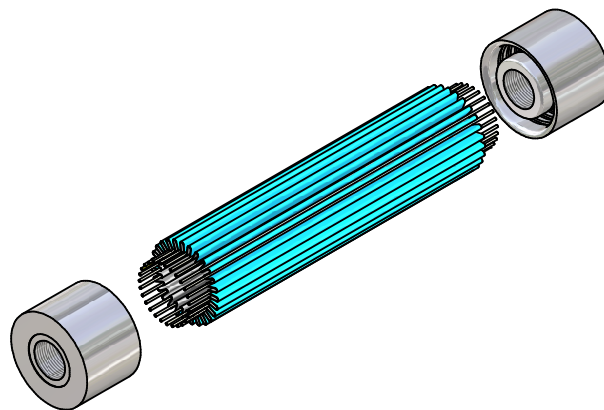


Figure 4: Composition of the new muscle prototype

Contrary to the former design, this muscle prototype does not incorporate air connectors. The end fittings have a treated hole in which additional muscle connectors can be screwed. An advantage of this setup is that a broken muscle can be replaced easily, without having to change the more complex muscle connectors. These connectors incorporate three functions: guiding the pressurized air in and out the enclosed volume, creating the interface for the connection to the specific application frame, and providing an attachment for a pressure sensor positioned inside the muscle. Figure 5 shows the two different connectors to be fixed at each side of the muscle.

The left side drawing of figure 5 shows the connector which allows the air to flow in and out of

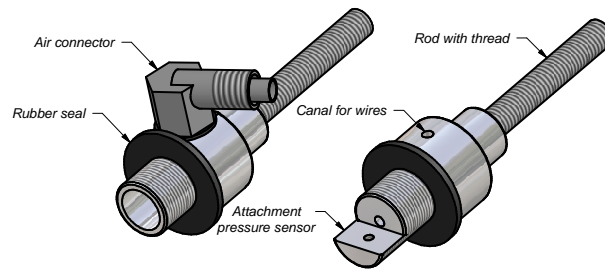


Figure 5: Drawing of the two muscle end connectors

the muscle, while the right side drawing depicts the connector with the attachment for a pressure sensor. Both connectors are made of aluminium and have a rubber sealing. At the back of each connector a threaded rod forms the interface to the application frame. In the muscle connector on the left of figure 5, a standard air tube connector can be fixed. In the muscle connector for the pressure sensor a small borehole has been drilled to guide the wires of the electronics needed for the pressure sensor, which is positioned inside the muscle. Once this sensor and its wiring are positioned, the borehole is filled with epoxy resin to prevent the air from escaping from the enclosed volume.



Figure 6: Photograph of inflated state of the second generation PPAM

Finally, figure 6 shows a photograph of the new muscle prototype. The muscle is shown in its inflated state. Note the regular unfolding of the flexible membrane while the Kevlar fibres stay positioned at equal distances. A lifespan test was performed, at which a muscle moves up and down a load of 130 kg by a slow varying gauge pressure between 1 and 3 bar. About 400.000 cycles have been reached before the test was ended. At this large number of cycles a few Kevlar fibres were broken somewhere in the end fittings. At these spots the epoxy resin makes the fibres fragile. Although movements of the fibres in the end fittings are small, due the large number of cycles, the fibres will break eventually. Although the reached number of cycles is already a significant improvement, currently, a third generation of muscle is being studied.

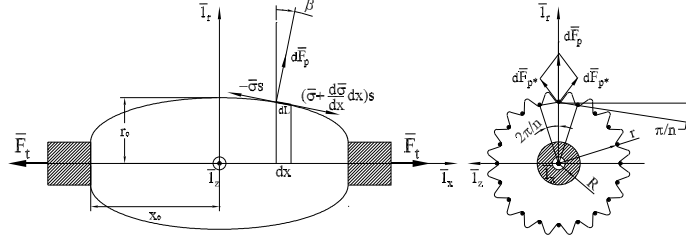


Figure 7: Meridional and parallel view of the PPAM

## 2.2 Mathematical model

In this section, the mathematical model describing the muscle characteristics, developed by [2], is adapted according to the new membrane design. The original model assumed a continuous axisymmetrical circular membrane, while for this model the focus lies on the discrete number of high tensile longitudinal fibres. The initial assumptions of the model are different, but the resulting analytical solution is almost identical. Therefore, only the starting point for the model is established here, while the elaboration on the analytical solution can be found in [2]. This PhD text can be found at the following website <http://lucy.vub.ac.be/publications.htm>.

In figure 7 a meridional and parallel section of the new muscle is given. The muscle is pressurized and subjected to a longitudinal traction force  $\bar{F}_t$ . For the mathematical formulation it is assumed that longitudinal tension is only transferred by the high tensile fibres which are positioned in each crease. Any influence of the more flexible longitudinal fibres of the airtight polyester membrane is thus neglected. The membrane transfers the forces  $\bar{F}_p$ , that are generated on it by the pressurized air, to the high tensile longitudinal fibres. In figure 8 a 3D-view of an infinitesimal section of the membrane is depicted with the forces acting on the longitudinal fibre.

At the left and right side of the fibre, part of the membrane transfers a force  $d\bar{F}_{p^*}$ . Due to the axisymmetrical situation of the closing membrane, the parallel components of these forces, which are tangent to the perpendicular circle running through the longitudinal fibres, compensate each other. Consequently, only the resultant force,  $d\bar{F}_p$ , is taken into account. The magnitude of this is calculated as:

$$|d\bar{F}_p| = 2p \cos \frac{\pi}{n} dA = 2pw \cos \frac{\pi}{n} dL \quad (2)$$

with  $p$  the gauge pressure inside the enclosed volume,  $n$  the number of longitudinal fibres, evenly distributed over the membrane,  $w$  representing half the distance between two neighbouring longitudinal fibres and  $dA$  the elementary surface associated with  $w$  and the infinitesimal section length  $dL$ . If  $\beta$  defines the oriented angle (counter-clockwise positive) between the radial direction  $\bar{I}_r$  and the force vector  $d\bar{F}_p$ , the components of this vector are represented by:

$$d\bar{F}_p = \left(-2pw \cos \frac{\pi}{n} dL \sin \beta\right) \bar{I}_x + \left(2pw \cos \frac{\pi}{n} dL \cos \beta\right) \bar{I}_r \quad (3)$$

$$= \left(-2pr \sin \frac{\pi}{n} \cos \frac{\pi}{n} \tan \beta dx\right) \bar{I}_x + \left(2pr \sin \frac{\pi}{n} \cos \frac{\pi}{n} dx\right) \bar{I}_r \quad (4)$$

$$= \left(-pr \sin \frac{2\pi}{n} \tan \beta dx\right) \bar{I}_x + \left(pr \sin \frac{2\pi}{n} dx\right) \bar{I}_r \quad (5)$$

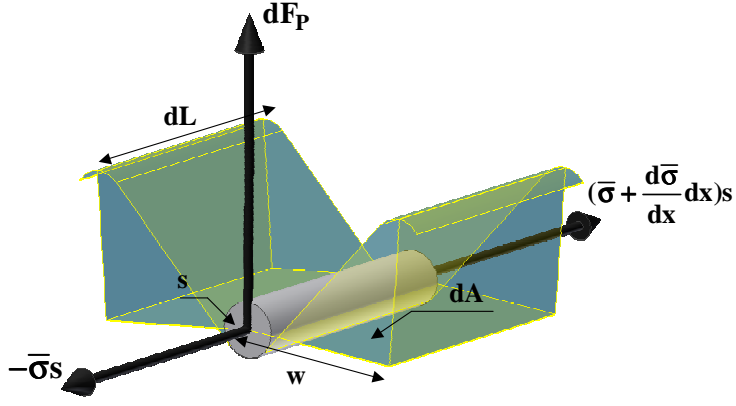


Figure 8: 3D-view of an infinitesimal section of the membrane

Hereby using following transformations:

$$\cos \beta = \frac{dx}{dL} \quad (6)$$

$$w = r \sin \frac{\pi}{n} \quad (7)$$

with  $r$  the radial distance from the fibre to the central muscle axis  $\bar{I}_x$  and  $dx$  the projection of the infinitesimal fibre length  $dL$  on to the same axis.

Assuming the tensile stress  $\sigma$ , generated in the high tensile longitudinal fibre, constant over the fibre section  $s$ , the force associated with this stress is given by:

$$\bar{\sigma}s = (\sigma s \cos \beta) \bar{I}_x + (\sigma s \sin \beta) \bar{I}_r \quad (8)$$

Shear stresses are neglected since the longitudinal fibre is extremely flexible in the perpendicular direction. If additionally the gravitational force associated with the weight of the membrane and high tensile fibres are neglected with respect to the much higher tensile forces, the equilibrium of forces acting on the infinitesimal fibre piece  $dL$  can be expressed along the directions  $\bar{I}_x$  and  $\bar{I}_r$ :

$$\bar{I}_x : \quad -pr \sin \frac{2\pi}{n} \tan \beta dx + \frac{d(\sigma s \cos \beta)}{dx} dx = 0 \quad (9)$$

$$\bar{I}_r : \quad pr \sin \frac{2\pi}{n} dx + \frac{d(\sigma s \sin \beta)}{dx} dx = 0 \quad (10)$$

Eliminating  $pr \sin \frac{2\pi}{n}$  from equations (9) and (10) leads to:

$$\frac{d(\sigma s \sin \beta)}{dx} \tan \beta + \frac{d(\sigma s \cos \beta)}{dx} = 0 \quad (11)$$

Rearranging the differentials and multiplying 11 with  $\cos \beta$  leads to:

$$\frac{d(\sigma s)}{dx} = 0 \quad (12)$$

which results in:

$$\sigma s = c \quad (13)$$

with  $c$  an integration constant.

And substituting  $\tan \beta = \frac{dr}{dx}$  in (9), while integrating gives:

$$\frac{r^2}{2} p \sin \frac{2\pi}{n} + c' = \sigma s \cos \beta \quad (14)$$

with  $c'$  an integration constant. Assuming that the traction force  $F_t$  is equally distributed over the  $n$  different longitudinal fibres, this integration constant can be interpreted as  $c' = \frac{F_t}{n}$  [2].

If the longitudinal high tensile fibres are assumed to be inelastic (a special case of the discussion in [2]) the following geometrical constraint on the fibre length  $l_0$  has to be taken into account:

$$\int_{x=0}^{x=x_0} dL = \int_{x=0}^{x=x_0} \sqrt{1 + \left(\frac{dr}{dx}\right)^2} dx = \frac{l_0}{2} \quad (15)$$

with  $x_0$  being the extreme ends of the enclosed volume of the muscle. Using the relation  $\sqrt{1 + \left(\frac{dr}{dx}\right)^2} = \frac{1}{\cos \beta}$  and  $c' = \frac{F_t}{n}$ , equation (14) can be transformed to the following differential equation:

$$dx = -\frac{c_2 r^2 + c_3}{\sqrt{1 - (c_2 r^2 + c_3)^2}} dr \quad (16)$$

with:

$$c_2 = \frac{p \sin \frac{2\pi}{n}}{2\sigma s} \quad (17)$$

$$c_3 = \frac{F_t}{n\sigma s} \quad (18)$$

Given a pressure  $p$  and traction  $F_t$ , as a consequence of equation (13),  $c_2$  and  $c_3$  are constant. Finally, the differential equation (16) can be integrated from  $x = 0$  to  $x(r)$ , in order to determine the shape of the curved fibres with each pressure level  $p$  and traction  $F_t$ . This integration is not straightforward but has been analytically described by Daerden. Only the solution is repeated here, a detailed discussion can be found in [2].

For the analytical solution two new constants,  $m$  and  $\varphi_R$  were introduced. These relate to  $c_2$  and  $c_3$  as follows:

$$c_2 = 2m \frac{\cos^2 \varphi_R}{R^2} \quad (19)$$

$$c_3 = 1 - 2m \quad (20)$$

and their values are bounded as ( $0 \leq m \leq 1/2$ ) and ( $0 \leq \varphi_R \leq \pi/2$ ). The symbol  $R$  represents the unpressurized muscle radius.

Defining the muscle contraction  $\epsilon$  as:

$$\epsilon = 1 - \frac{2x_0}{l_0} \quad (21)$$

and after introducing the running coordinate  $\varphi$ , the shape of the longitudinal fibres, at contrac-

tion  $\epsilon$ , can be found from the following set of equations:

$$x = \frac{R}{\sqrt{m} \cos \varphi_R} \left( E(\varphi \setminus m) - \frac{1}{2} F(\varphi \setminus m) \right) \quad 0 \leq \varphi \leq \varphi_R \quad (22)$$

$$r = \frac{R}{\cos \varphi_R} \cos \varphi \quad 0 \leq \varphi \leq \varphi_R \quad (23)$$

$$\frac{E(\varphi_R \setminus m) - \frac{1}{2} F(\varphi_R \setminus m)}{\sqrt{m} \cos \varphi_R} = \frac{l_0}{2R} (1 - \epsilon) \quad (24)$$

$$\frac{F(\varphi_R \setminus m)}{\sqrt{m} \cos \varphi_R} = \frac{l_0}{R} \quad (25)$$

with  $E(\varphi \setminus m)$  and  $F(\varphi \setminus m)$  elliptical integrals of the first and second kind.

For each contraction  $\epsilon$ , a combination of the constants  $m$  and  $\varphi_R$  have to be calculated from equations (24) and (25). With these values, equations (22) and (23) fully characterize the shape  $x(\varphi) - r(\varphi)$  of the fibres at each contraction. From this set of equations, valid only with the assumption of inelastic fibres, it is seen that the solution is characterized by the muscle slenderness  $l_0/R$ . At this point there is no difference with the solution of Daerden, the shape at which the longitudinal fibres position at each contraction  $\epsilon$  is the same. The difference arises when expressing the force generated with each contraction. This force is dependent on the number of fibres as is shown in the next section.

### 2.3 Characteristic of the PPAM

Daerden [2] extensively discusses several characteristics concerning the PPAM, for inelastic as well as elastic membranes. Hereby giving for each contraction the characteristics of the membrane shape, muscle traction, enclosed volume, maximum muscle diameter, and fibre stress and strain values. Here two important characteristics are discussed: generated traction and enclosed volume for each contraction. The first is used for joint torque dimensioning and control purposes, while the latter can be important for simulation purposes and calculation of joint compliance with closed muscles.

To determine the traction characteristics, equations (17) and (18) are combined with the parameter transformations (19) and (20):

$$F_t = n \sigma s c_3 = pn \sin \left( \frac{2\pi}{n} \right) \frac{c_3}{2c_2} = pn \sin \left( \frac{2\pi}{n} \right) \frac{(1-2m)R^2}{4m \cos^2 \varphi_R} \quad (26)$$

And using equation (24) gives:

$$F_t = pn \sin \left( \frac{2\pi}{n} \right) l_0^2 \frac{(1-2m)(1-\epsilon)^2}{16 [E(\varphi_R \setminus m) - \frac{1}{2} F(\varphi_R \setminus m)]^2} \quad (27)$$

$$= p \frac{n}{2\pi} \sin \left( \frac{2\pi}{n} \right) l_0^2 f \left( \epsilon, \frac{l_0}{R} \right) \quad (28)$$

with  $f \left( \epsilon, \frac{l_0}{R} \right)$  the dimensionless force function as defined by [2]. Expression (28) shows the difference between the current model and the one of Daerden, namely a term  $\frac{n}{2\pi} \sin \frac{2\pi}{n}$  appears. This term lowers the generated traction compared to the model of Daerden when the number of fibres is decreased. When increasing the number of fibres, the difference between the traction

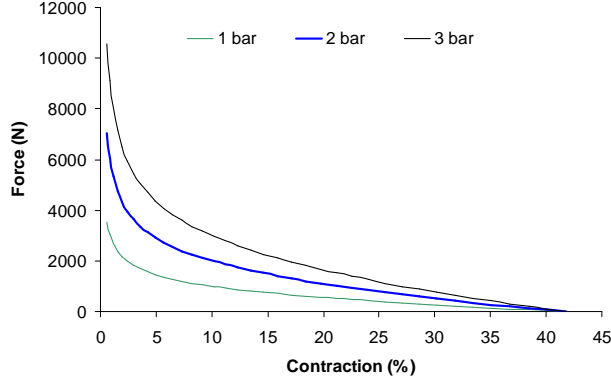


Figure 9: Theoretical forces at pressure levels 1, 2 and 3 bar as a function of contraction

models becomes smaller. As the number of used fibres ( $n$ ) increase to infinity, the model should corresponds to the case of a closed circular membrane, as was assumed by Daerden:

$$\lim_{n \rightarrow \infty} \frac{n}{2\pi} \sin \frac{2\pi}{n} = 1 \quad (29)$$

Thus the two models are the same for large numbers of discrete fibres. The limit in equation 29 converges fast to 1, if the number of used fibres is greater then 15 the difference between the two models is less then 3 %. Generally, if the number of fibres is large enough, the generated muscle force depends on the applied gauge pressure ( $p$ ), the contraction ( $\epsilon$ ) and the two parameters, initial muscle length ( $l_0$ ) and slenderness ( $\frac{l_0}{R}$ ). The latter two are important during the joint design process, where these parameters are chosen as a function of the desired joint torque characteristics.

For the mathematical description of the enclosed volume, the pleated polyester membrane is approximated by considering at each parallel section a circular membrane pattern instead of the pleated structure. These calculations are identical as in the work of [2] and resulted in the following expression:

$$V = l_0^3 v \left( \epsilon, \frac{l_0}{R} \right) \quad (30)$$

with  $v$  a dimensionless function of the contraction and the slenderness only.

Tested muscles which are currently used for several setups have a physical membrane length  $l_0 = 110$  mm and an unpressurized radius  $R = 11.5$  mm for the position of the Kevlar fibres and a radius of 16 mm at the top of the polyester fabric pleats. These specific dimensions result from the standard tools used for the fabrication of the muscles, and the unloaded radius takes into account the dimensions of the pressure sensor which is positioned inside the muscle. The muscle used for the biped is constructed with 40 aligned fibre yarns. The extra term (29), distinguishing this specific force model, is 0.996 for this number of fibres. So the predicted forces generated by this muscle are almost identical for both models. Using  $l_0 = 110$  mm,  $R = 11.5$  mm and  $n = 40$  in equation (28), results in the force characteristics depicted in figure 9. The traction as a function of contraction is drawn for different applied gauge pressures: 1, 2 and 3 bar. The graph shows the nonlinear character of the generated muscle force. For small contractions, the forces are extremely high, while for large contractions, the forces drop to zero. For the practical robot application, contractions will be bounded somewhere between 5 and 35 %. The first limit is set to bound the stresses on the fibres and consequently extend the lifetime of the muscle. And beyond 35 % contraction, forces drop too low to be of practical use. In figure 10 the volume

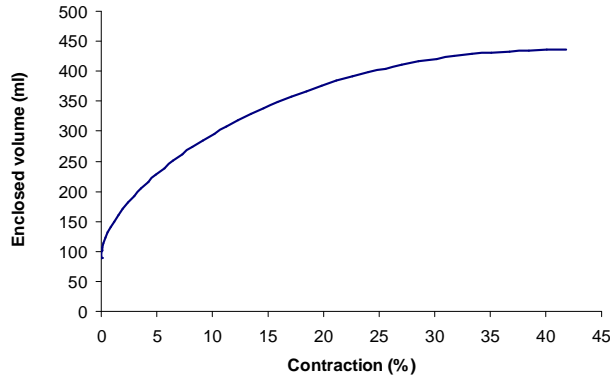


Figure 10: Theoretical enclosed muscle volume as a function of contraction

characteristic is given for the considered muscle dimensions. The volume ranges from a dead volume of approximately 100 ml at zero contraction to a volume of about 400 ml at maximum contraction. To the dead volume, the volumes of the end fittings and tubing should be added.

### 3 Static load tests

Static load tests on real muscles are carried out to validate the proposed mathematical model of equation (28). Three different muscles are tested with an Intron test bench (model 4505) at isobaric conditions, while applying three different gauge pressures: 1, 2 and 3 bar. The forces are recorded with a load cell of 10 kN (accuracy  $\pm 0.05\%$ ) and the pressure inside the muscle is regulated with a Kolvenbach pressure servo-valve, KPS3/4. In order to increase accuracy, the pressure inside the muscle is separately measured with a silicon gauge pressure sensor, XCA5-60GN, from Data Instruments (accuracy  $\pm 0.5\%$  of 60 psi span). This sensor is placed as close as possible to the inlet of the muscle. One side of the muscle is fixed to the load cell, while the other side is attached to a movable frame. The tests are performed by changing the displacement of this frame. During each test, frame position, muscle force and applied gauge pressure are recorded.

For each test, the voltage controlling the servo-valve is set at the beginning of each run to regulate the pressure in the muscle for a constant level. Subsequently, the moving part of the test bench displaces in such a way that the generated force of the muscle ranges between 100 N and 3000 N, hereby following a slow sine-wave path of 0.005 Hz such that the pressure is stabilized at each measurement. Figure 11 gives the results of these tests by depicting force as a function of contraction for each of the three muscles at the three different gauge pressures. Although the muscles are handmade, the repeatability is very satisfactory. On the graph, an un-modelled hysteresis effect on the actual force as a function of contraction curve is noticed. It is seen that the different curves show a more or less comparable hysteresis width. Due to the pressure regulating valve, the actual pressure during each test run is not exactly the same. To overcome this, it is better to compare the test results by dividing the measured forces by the measured pressures. Figure 12 shows all the pressure scaled measurements together with estimated theoretical force functions of equation (28). These two theoretical graphs are calculated with  $R = 11.5$  mm and  $R = 16$  mm respectively. The first compares to the actual radius at which the Kevlar fibres are positioned during construction of the muscles. The radius equal to 16 mm corresponds to the radius of the top of the pleats, which is the same as the outer radius of the enclosed volume at

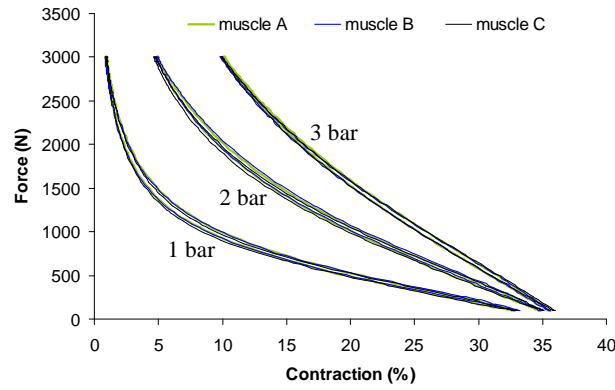


Figure 11: Measured forces as a function of contraction for three muscles at pressure levels 1, 2 and 3 bar

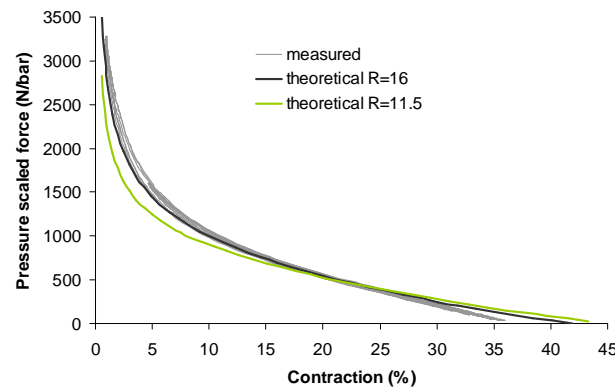


Figure 12: Pressure scaled measured forces as a function of contraction compared with theoretical model

the aluminium end fittings. It is seen that the theoretical model with  $R = 11.5$  mm does not fit the measured data, while the other graph with  $R = 16$  mm is much more suited to represent the actual generated force. Since the epoxy resin reaches to only about a centimeter away from the edge of the end fitting, the Kevlar fibres tend to be positioned at the outer radius of the aluminium basin, immediately after the muscle is pressurized. At all contractions the fibres at the end fittings stay at this radius, as if the initial radius was  $R = 16$  mm. This explains why the theoretical function with the larger radius fits the measured data much better. For full bulging of the muscle the initial diameter of the cylindrical polyester membrane should be taken higher than the initial length of the muscle. But it has been observed, for a muscle with not fully unfolded pleats at maximum contraction, that the unfolding process is less regular as with the previous muscle design. So the initial diameter of the cylindrical polyester tube is taken smaller. Consequently, the muscle can not fully bulge and at certain contraction level, radial stresses in the polyester membrane start influencing the traction characteristic. This explains why the theoretical model deviates from the measured data (see figure 12) at large contractions.

Since the force functions of the different muscles are very similar, a polynomial function fit on the pressure scaled measured data is performed in order to achieve a better force estimation. The nonlinear nature of the force function attains extremely large values at small contractions, therefore it is more suitable to perform a polynomial fit on the scaled force function multiplied with contraction. This lowers after all the extreme values at small contractions. A 4th order polynomial fit on these data is performed. With the incorporation of pressure  $p$  and the square

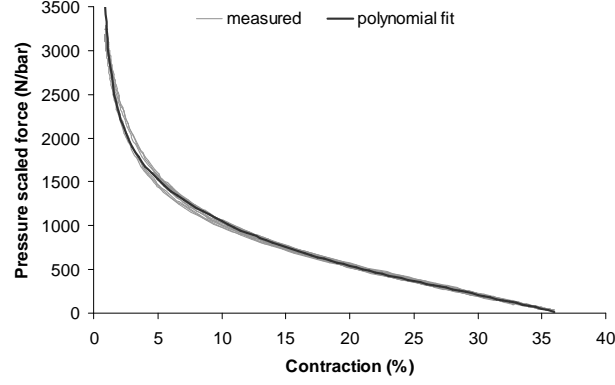


Figure 13: Pressure scaled measured forces as a function of contraction compared with polynomial fitted estimation

of the initial muscle length  $l_0^2$ , as was described by the theoretical model, the polynomial fit of the force function can be expressed as:

$$F_t = pl_0^2 f(\epsilon) = pl_0^2 (f_4 \epsilon^3 + f_3 \epsilon^2 + f_2 \epsilon + f_1 + f_0 \epsilon^{-1}) \quad (31)$$

with  $f_0$  to  $f_4$  the 5 coefficients resulting from a 4th order polynomial approximation. Figure 13 shows all the pressure scaled force measurements in comparison with the estimated force function. The coefficients of the fitting process for the force function, following the structure of equation (31), are given in table (1). The values are valid when the generated force  $F_t$  is expressed in N, the initial muscle length  $l_0$  in m, the pressure expressed in bar and the contraction  $\epsilon$  expressed in %.

$f_4$	$f_3$	$f_2$	$f_1$	$f_0$
-2.0413	171.623	-7178.93	128611.6	146099

Table 1: Coefficients of the polynomial force function approximation

Finally, a polynomial fitting is performed on the theoretical data for the enclosed muscle volume depicted in figure 10:

$$V(\epsilon) = l_0^3 v(\epsilon) = l_0^3 (v_5 \epsilon^5 + v_4 \epsilon^4 + v_3 \epsilon^3 + v_2 \epsilon^2 + v_1 \epsilon + v_0) \quad (32)$$

with  $v_0$  to  $v_5$  the 6 coefficients resulting from a 5th order polynomial approximation. Equation (32) is much easier to handle than the numerical solution derived from the mathematical model represented by expression (30). In table 2 the coefficients of the volume fitting, following equation (32), are given. The values are valid for the volume given in ml, the initial length expressed in m and the contraction  $\epsilon$  expressed in %. The data in table 1 and 2, together with equations (31) and (32), can also be used to generate an approximation of the force and volume characteristics for muscles with lengths different from  $l_0 = 110$  mm. But the values in these tables are only valid for muscles with a specific slenderness ( $l_0/R = 110/16 = 6.9$ ), as is explained by the theoretical

$v_5$	$v_4$	$v_3$	$v_2$	$v_1$	$v_0$
0.02254	-2.6296	113.82	-2386.3	30080	71728

Table 2: Coefficients of the polynomial volume function fitting

model with equations (30) and (28). So, whenever the polynomial fitting is used for a muscle with different initial length, the unloaded radius of that muscle has to be adapted, otherwise the force and volume approximations are not valid.

## 4 Applications of the PPAM

### 4.1 The PPAM for legged robots

Not so long ago legged robots were exclusive topics for science-fiction movies and the imagined world of children. But recent developments indicate that these machines will become full-fledged robots in near future. One example is the Honda Motor Corporation, that developed the Honda Human Robot followed by its successors P1, P2 and recently ASIMO focusing on the field of domotics. In the leisure industry the Sony company already made one commercially available four legged robot, AIBO, and has created a humanoid robot QRIO. But also legged robots for industrial use are increasingly gaining interest, e.g., the Spanish climbing robots for the maritime industry. Since a few years the Japanese government together with most of the leading Japanese manufacturers are investing heavily in the HRP-project. This project tries to create ready-to-use industrial, domotic and health-care applications for humanoid robots.

But in spite of the magnificent models already created a lot of research in many different fields ranging from artificial intelligence to mechanical design is still needed. One of the topics is the implementation of novel actuators, such as the PPAM, replacing the widely spread electrical drives, in order to make lightweight structures and compliant joints. Compliance characteristics can be used to reduce impact and energy consumption.

The Biped "LUCY" is a two dimensional walking robot with two articulated legs and a armless body. This robot has been built to create a test bed for the evaluation of the PPAM implemented in legged robots. This research is focused on the exploitation of the adaptable compliance present in a joint actuated by two artificial muscles. One can show that joint position is determined by pressure differences in both muscles while the stiffness of a joint is characterized by the sum of pressures. This means that stiffness can be changed while still controlling position. The adaptability of compliance is very important regarding energy consumption and control efforts. The strategy is to select appropriate stiffness parameters in the different joints in order to adapt the natural dynamics of the robot to an imposed desired motion. Moving within the natural dynamics of a system would only need energy to overcome friction, while each motion deviating from this situation would require more energy input and control effort.

Figure 14 shows a picture of Lucy, more information about this biped can be found in [20] and movies can be viewed at the Lucy website <http://lucy.vub.ac.be/>.

### 4.2 The PPAM in a Manipulator Application

Repetitive manual handling of heavy loads is common in assembly and is a frequent cause of lower back disorders. This can have a significant impact on the quality of life and has a serious economic cost. Manipulators are robotic systems designed to avoid these problems. They assist people in performing heavy-duty tasks. Most of the commercially available manipulators use a counterweight, which limits their use to handling loads of a specific mass. Others are electrically



Figure 14: Picture of the robot Lucy, actuated by 12 PPAM

or hydraulically actuated. This usually makes them heavy, complex and expensive. The use of the PPAM actuator allows us to tackle these issues and develop a manipulator that combines ergonomics, operator safety, low cost, low weight and ease of operation.

The goal of this research is to develop a manipulator that will be used in direct contact with an operator, without expensive force or torque sensors and without user interaction through control elements (such as joysticks). The system should behave as follows: when the operator wants to move a load attached to the manipulator, he/she starts moving it as if there were no manipulator. By measuring the muscle gauge pressures, the system can estimate the forces applied by the operator and assist him in accomplishing the desired load movement. Ideally, moving a 30 kg load would feel like moving a 3 kg load. The direct interaction between operator and load (without intermediary control tools) allows for precise positioning.

The main requirement for any mechanical device that is used in the immediate environment of people is safety. The PPAM actuators greatly contribute to the overall safety of the manipulator system: they allow for a lightweight construction, there is no danger of electrocution and, most important of all, the muscles are inherently compliant. The controller will also enhance safety, since there is no fundamental difference between forces generated by a collision and forces applied by an operator. The system will always tend to move away from people or objects it collides with.

A hardware setup of a small-scale manipulator is constructed. It consists of two PPAM actuated links in inverse elbow configuration. A picture of the manipulator arm is given in figure 15. More information about this research can be found in [21] and some movies can be found at the website <http://softarm.vub.ac.be/>.



Figure 15: Picture of the manipulator arm, actuated by 4 PPAM

## 5 Summary

In this paper the pleated pneumatic artificial muscle, as designed by Daerden was introduced. This type of artificial was developed to overcome dry friction and material deformation which is present in the widely used McKibben type of artificial muscle. The essence of the PPAM is its pleated membrane structure which enables the muscle to work at low pressures and at large contractions. In order to deal with some limitations of the PPAM design of Daerden, a second generation of PPAM was proposed. A redesign of the pleated membrane structure resulted in a much higher muscle lifespan which is an essential property if the muscle is used for an elaborate experimental setup. Additionally, some changes made to the end fitting design simplified machining of the muscle and provided possible reuse of some muscle parts.

The new membrane layout differs from the previous design mainly due to usage of a discrete number of high tensile fibres instead of a complete high tensile stiff fabric. Therefore the mathematical model of the muscle, introduced by Daerden, was reformulated. This model describes the shape of the muscle bulging at each contraction, and gives essential characteristics such as muscle traction and enclosed volume. The difference in the adapted mathematical model is seen in the formulation for the generated muscle force, which becomes dependent on the discrete number of high tensile fibres used to contract the muscle.

In order to validate the theoretical traction function with the real force generation, static load tests on a specific muscle were carried out. It was found that the mathematical model gives a good approximation for the force function such that it can be used for dimensioning purposes. Additionally, a polynomial fit on the measured force data was carried out to have a more accurate force estimate.

Recently, there is a growing interest for the use of pneumatic artificial muscles for robotic application due to the high power to weight ratio and the adaptable compliance. Two applications which incorporate the PPAM have been given. One is the biped Lucy, in which the adaptable joint compliance is used in order to exploit the natural dynamics of the system. Another application is a manipulator arm in which the compliance is very important since this manipulator is working in direct contact with an operator. A another interesting application for pneumatic artificial muscles lies in the field of prostheses and orthoses.

## References

- [1] C.-P. Chou and B. Hannaford, "Measurement and modeling of McKibben pneumatic artificial muscles," *IEEE Transactions on Robotics and Automation*, vol. 12, no. 1, pp. 90–102, 1996.
- [2] F. Daerden, *Conception and Realization of Pleated Pneumatic Artificial Muscles and their Use as Compliant Actuation Elements*. PhD thesis, Vrije Universiteit Brussel, 1999.
- [3] G. B. Immega, "ROMAC actuators for micro robots," in *Proceedings of the IEEE Micro Robotics and Teleoperators Workshop*, (Hyannis, Massachusetts), 1987.
- [4] H. A. Baldwin, "Realizable models of muscle function," in *Proceedings of the First Rock Biomechanics Symposium*, (New York, USA), pp. 139–148, 1969.
- [5] N. Saga, T. Nakamura, J. Uehara, and T. Iwada, "Development of artificial muscle actuator reinforced by kevlar fiber," in *Proceedings of IEEE International Conference on Industrial Technology*, (Bangkok, Thailand), pp. 950–954, 2002.
- [6] H. F. Schulte, "The characteristics of the McKibben artificial muscle," in *The Application of External Power in Prosthetics and Orthotics*, no. Publication 874, pp. 94–115, Lake Arrowhead: National Academy of Sciences–National Research Council, 1961.
- [7] K. Inoue, "Rubbertuators and applications for robotics," in *Proceedings of the 4th International Symposium on Robotics Research*, pp. 57–63, 1987.
- [8] Shadow Robot Company, "Design of a dextrous hand for advanced CLAWAR applications," in *Proceedings of the 6th International Conference on Climbing and Walking Robots and the Support Technologies for Mobile Machines*, (Catania, Italy), pp. 691–698, 2003.
- [9] Merlin Systems Cooperation, "Merlin actuators: Automation, animatronics and artificial creatures," *Brochure Merlin Actuators*, 2003.
- [10] Festo, "Fluidic muscle MAS," *Festo Brochure Fluidic Muscle*, 2004.
- [11] T. Raparelli, G. Mattiazzo, S. Mauro, and M. Velardocchia, "Design and development of a pneumatic anthropomorphic hand," *Journal of Robotic Systems*, vol. 17, no. 1, pp. 1–15, 2000.
- [12] S. Eskiizmiler, B. Tondu, and C. Darlot, "Motor control of a limb segment actuated by artificial muscles," in *Proceedings of the 23th IEEE/EMBS Annual Conference*, (Istanbul, Turkey), 2001.
- [13] K. G. Klute, J. M. Czerniecki, and B. Hannaford, "Artificial muscles: Actuators for biorobotic systems," *The International Journal of Robotics Research*, vol. 21, no. 4, pp. 295–309, 2002.
- [14] K. Berns, J. Albiez, V. Kepplin, and C. Hillenbrand, "Airbug insect-like machine actuated by fluidic muscle," in *Proceedings of the 4th International Conference on Climbing and Walking Robots, from Biology to Industrial Application*, (Karlsruhe, Germany), pp. 237–244, 2001.
- [15] S. Davis, N. Tsagarakis, J. Canderle, and D. Caldwell, "Enhanced modelling and performance in braided pneumatic muscle actuators," *The International Journal of Robotics Research*, vol. 22, no. 2-3, pp. 213–227, 2003.

- [16] D. A. Kingsley, R. D. Quinn, and R. E. Ritzmann, "A cockroach inspired robot with artificial muscles," in *Proceedings of the International Symposium on Adaptive Motion of Animal and Machines*, (Kyoto, Japan), 2003.
- [17] P. Pomiers, "Modular robot arm based on pneumatic artificial rubber muscles (PARM)," in *Proceedings of the 6th International Conference on Climbing and Walking Robots and the Support Technologies for Mobile Machines*, (Catania, Italy), pp. 879–886, 2003.
- [18] K. Kawashima, T. Sasaki, T. Miyata, M. Nakamura, N. Sekiguchi, and T. Kagawa, "Development of robot using pneumatic artificial rubber muscles to operate machinery," *Journal of Robotics and Mechatronics*, vol. 16, no. 1, pp. 8–16, 2004.
- [19] M. Wisse, *Essentials of Dynamic Walking : Analysis and Design of Two-Legged Robots*. PhD thesis, Technische Universiteit Delft, 2004.
- [20] B. Verrelst, R. Van Ham, B. Vanderborght, F. Daerden, D. Lefeber, and J. Vermeulen, "The pneumatic biped "lucy" actuated with pleated pneumatic artificial muscles," *Autonomous Robots*, vol. 18, pp. 201–213, 2005.
- [21] M. Van Damme, F. Daerden, and D. Lefeber, "Design of a pneumatic manipulator in direct contact with an operator," in *Proceedings of the 35th International Symposium on Robotics*, (Paris, France), 2004.